Journal of Catalysis 275 (2010) 11–24

Contents lists available at ScienceDirect

Journal of Catalysis

journal homepage: www.elsevier.com/locate/jcat

Surface-functionalized TUD-1 mesoporous molecular sieve supported palladium for solvent-free aerobic oxidation of benzyl alcohol

Yuanting Chen, Zhen Guo, Tao Chen, Yanhui Yang *

School of Chemical and Biomedical Engineering, Nanyang Technological University, Singapore 637459, Singapore

ARTICLE INFO

Article history:
Received 5 April 2010
Revised 5 June 2010
Accepted 3 July 2010
Available online 16 August 2010

Keywords:
Benzyl alcohol oxidation
Palladium
TUD-1
Surface functionalization

ABSTRACT

Palladium catalysts supported on TUD-1 mesoporous molecular sieves functionalized with various organosilanes were successfully prepared using a post-synthesis grafting method combined with a metal adsorption–reduction procedure. The correlation between catalyst structure, surface chemistry, metal loading, and catalytic activity was explored in the solvent-free selective oxidation of benzyl alcohol using molecular oxygen. TUD-1 outperformed other mesoporous silicas due to its unique open 3-D sponge-like mesostructure, which can effectively confine Pd nanoparticles and suppress the mass diffusion resistance. The type and content of grafted functional groups greatly affected the catalytic performance by tuning the surface basicity, metal particle size and size distribution, and metal–support interaction. 3-Aminopropyl triethoxysilane functionalization displayed the largest improvement in catalytic activity, showing a dramatically high quasi-turnover frequency of 18,571 h^{-1} for benzyl alcohol conversion.

1. Introduction

Making aldehydes or ketones from the selective oxidation of corresponding alcohols, in particular, benzaldehyde from benzyl alcohol is regarded as one of the most versatile and powerful reactions in organic synthesis on both the laboratory and industrial scales. The catalytic roles of heterogenized noble metal (Pd, Au, Pt, Ru) catalysts in the aerobic oxidation of benzyl alcohol have been extensively investigated due to their superior catalytic performance relative to non-noble metals [1]. Among these noble metals, palladium catalysts have attracted considerable attention and been intensively studied. Numerous authors have reported the investigations into Pd-heterogeneous catalysts since the first successful Pd catalyzed aerobic oxidation of secondary alcohols [2]. Mori et al. showed that supported Pd catalysts are highly effective for the oxidation of 1-phenylethanol under mild solvent-free conditions, showing a turnover frequency (TOF) of 9800 h^{-1} for Pd supported on hydroxyapatite (Pd/HAP) [3]. Li et al. reported that zeolite-supported Pd nanoparticles with a mean diameter of 2.8 nm exhibited an extraordinary TOF of 18,800 h^{-1} for 1-phenylethanol oxidation [4].

A strong alkaline medium is beneficial for certain reactions, and it has been demonstrated that gold alone cannot catalyze alcohol dehydrogenation in the absence of a strong base [5]. Basicity also plays a crucial role in the selective oxidation of alcohols, especially for primary alcohols. Precisely, controlling the alkaline pH level in the reaction solution is vital to enhance the reaction by facilitating the reactant adsorption and product desorption, leading to a good-to-excellent selectivity [6]. Alternatively, base can be added to a heterogeneous catalyst as the promoter, enhancing the hydrogen abstraction from –OH groups which is proposed as the rate-limiting step [7]. Klitgaard et al. also suggested that base additives suppressed the catalyst deactivation and restored the catalyst activity in benzyl alcohol oxidation by diminishing the free benzoic acid level in the reaction solution [8]. Zhu et al. identified that the role of base was to provide OH^- anions to form Au–OH^- sites for the H-abstraction step, which was difficult by using only gold as the active sites [9]. Nevertheless, adding alkaline agents (either tuning the pH in reaction solution or adding promoters to the catalyst) brings several drawbacks: the metal catalyst may dissolve at high pH and be leached out [6]; the base promoter is also susceptible to leaching during the reaction, and side reactions could be provoked, e.g., keto-enol equilibration, Cannizzaro reaction, and oxidative decarbonylation [10].

Nowadays, chemical functionalization of catalyst support using a base modifier via the post-synthesis grafting method has been employed as a promising alternative to the addition of alkaline metal hydroxide and cations. Many silane modifiers can be selected to functionalize the support surface to obtain the "customized" surface properties. In addition, these immobilized organic functional groups, such as thiol and amino groups, act as anchoring sites to facilitate the stabilization of metal nanoparticles, which are mobile and prone to sinter on the support surface [11]. Development of surface-functionalized catalysts for selective alcohol oxidation has been reported [12]. The localized basicity on the support

* Corresponding author. Fax: +65 6794 7553.
E-mail address: yhyang@ntu.edu.sg (Y. Yang).

0021-9517/$ - see front matter © 2010 Elsevier Inc. All rights reserved.
doi:10.1016/j.jcat.2010.07.006

surface is able to accelerate the alcohol dehydrogenation, suppress side reactions, and enhance the desorption of products without significantly elevating the solution pH [13]. Hu et al. successfully confined highly dispersed Au nanoparticles on the surface of functionalized silica materials, showing a 100% conversion in the benzyl alcohol oxidation [14].

Our laboratory has previously reported both highly dispersed Au monometallic and Au–Pd bimetallic nanoparticles confined in surface-functionalized SBA-16 as good catalytic materials for the selective oxidation of benzyl alcohol [15,16]. Nevertheless, limited enhancement of catalytic activity was found and attributed to the mass transfer restriction. A recent addition to the mesoporous material family is the so-called TUD-1 mesoporous silica [17]. In the synthesis of TUD-1, surfactant and/or block co-polymer are replaced by inexpensive triethanolamine molecules as the structure-directing agent. Interestingly, the unique open 3-D sponge-like wide mesoporous structure of TUD-1 can effectively decrease the pore diffusion resistance as we previously demonstrated [18]. Herein, we synthesize and characterize a series of Pd catalysts supported on TUD-1 mesoporous silicas functionalized with several organic functional groups, especially amino groups. The aerobic oxidation of benzyl alcohol in the absence of any inorganic base is employed as a model reaction to evaluate these as-synthesized Pd catalysts. The catalytic activity will be benchmarked against Pd catalysts supported on other mesoporous silicas, e.g., MCM-41, SBA-15, and SBA-16. The correlation between catalyst structure, surface chemistry, metal loading, and catalytic activity will be explored and discussed in detail.

2. Experimental

2.1. Chemicals

Tetraethyl orthosilicate (TEOS, 98%, Aldrich), triethanolamine (TEA, >98.5%, Fluka), tetraethyl ammonium hydroxide (TEAOH, 35%, Aldrich), (3-aminopropyl)triethoxysilane (APS, ⩾98%, Sigma–Aldrich), [3-(2-aminoethylamino)propyl]trimethoxysilane (ATMS, 97%, Aldrich), hexamethyldisilazane (HMDS, Sigma), (3-mercaptopropyl)trimethoxysilane (MPTMS, Aldrich), palladium chloride ($PdCl_2$, Sigma–Aldrich), benzyl alcohol (98%, Sigma) were used as received without any further pretreatment.

2.2. Synthesis

TUD-1 was synthesized following the hydrothermal method reported by Quek et al. [18], using TEA and TEOS as template and silica precursor, respectively. The preparation procedures were as follows: 7.2 g of TEA and 1.8 g of deionized water were added drop wise to 10.0 g of TEOS under vigorous stirring. After 30 min, 10.1 g of TEAOH was added. The mixture was aged at room temperature for 24 h, dried at 100 °C for 24 h, and hydrothermally treated in a Teflon-lined stainless steel autoclave at 180 °C for 8 h. The final product was calcined at 600 °C for 10 h in air to remove the template. MCM-41 and SBA-15 were synthesized following the methods reported by Chi et al. [19]; and SBA-16 was prepared following the procedure reported by Kleitz et al. [20].

TUD-1, as well as other mesoporous silica materials surface functionalized with organosilanes (APS, ATMS, HMDS, and MPTMS), was successfully prepared via a post-synthesis grafting method, as illustrated in Scheme 1. In a typical preparation as exemplified by APS-modified TUD-1, 1.0 g of TUD-1 was dispersed in 30 mL of toluene and refluxed at 110 °C for 12 h under a N_2 flow of 50 mL min^{-1}. Then, 1.2 mmol of APS (or an appropriate amount of other silane modifiers) was added to the suspension and stirred for another 5 h. The resulting powders were filtered, washed with toluene, and dried at 80 °C to remove the remaining solvent. The corresponding samples were denoted as APS-TUD, ATMS-TUD, HMDS-TUD, and MPTMS-TUD.

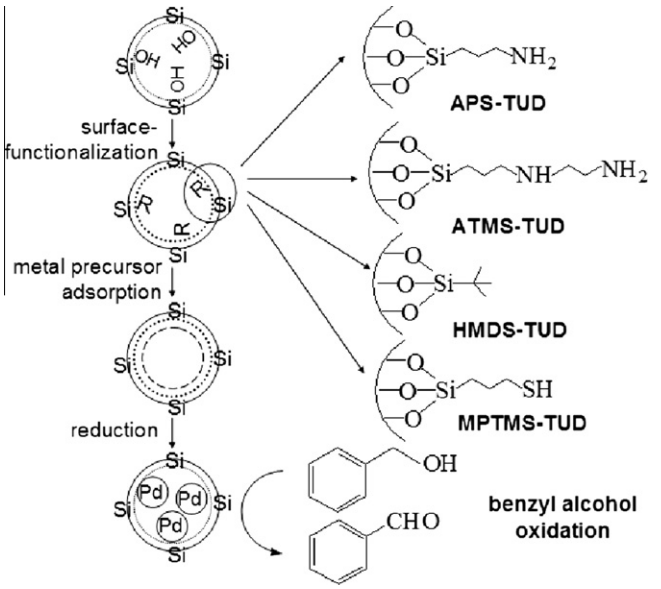

Scheme 1. Preparation procedures and catalytic evaluation of surface-functionalized TUD-1-supported Pd catalysts.

Palladium catalysts supported on surface-functionalized TUD-1 were prepared by an adsorption–reduction method reported by Chi et al. [19]. A volume of 375.9 μL of 0.05 M $PdCl_2$ aqueous solution was added to 0.2 g of surface-functionalized TUD-1, e.g., APS-TUD, suspended in 20 mL deionized water, followed by vigorous stirring at 80 °C for 5 h. The catalyst, donated as Pd/APS-TUD, was obtained by filtering and washing with deionized water, and drying at 80 °C overnight. The catalyst was pretreated in a H_2 flow of 20 mL min^{-1} at 400 °C for 2 h to reduce Pd cations to Pd metal nanoparticles.

2.3. Characterizations

Nitrogen physisorption isotherms were measured at −196 °C on a static volumetric instrument Autosorb-6b (Quanta Chrome). Prior to each measurement, the sample was degassed at 250 °C for 12 h under high vacuum. The specific surface area was estimated by the Brunauer–Emmett–Teller (BET) method [21], and the pore size distribution was calculated by the Barrett–Joyner–Halenda (BJH) method [22] using the desorption isotherm branch. Powder X-ray diffraction (XRD) patterns were recorded on a Bruker AXS D8 diffractometer (under ambient conditions) using filtered Cu Kα radiation (λ = 0.15406 nm) operated at 40 kV and 40 mA. Diffraction data were collected from 30 to 80° with a resolution of 0.01° (2θ). Prior to a test, sample was dried at 100 °C overnight. Transmission electron microscopy (TEM) was performed on a JEOL JEM-2100F, operated at 200 kV. The sample was suspended in ethanol and dried on holey carbon-coated Cu grids. The metal content was measured by inductively coupled plasma (ICP), 40% hydrofluoric acid was used to dissolve the sample. The pH of pristine and functionalized TUD-1 supports with different organic groups was measured following the method reported by Tian et al. [23]. A concentration of 0.2 mg of dry sample was added to 10 mL of hot fresh distilled water, boiled for 5 min, cooled to room temperature, and stirred overnight to reach equilibrium. The suspension was filtered and the pH of the filtrate was measured by a pH meter.

UV–vis–NIR diffuse reflectance spectra were collected on a Varian-Cary 5000 UV–vis–NIR spectrophotometer equipped with

a diffuse reflectance accessory. The spectra were recorded in the range of 1000–2500 nm at room temperature with $BaSO_4$ as a reference. All samples were dried at 100 °C overnight before conducting the test. Fourier Transform Infrared (FTIR) spectra were recorded on a PerkinElmer Spectrum One FT-IR spectrometer at room temperature with KBr pellets (4000–450 cm^{-1}, resolution of 1 cm^{-1}). The in situ infrared reflection absorption spectroscopy (IRAS) was collected on the same equipment using CO as probe molecules. The sample was pressed into pellet with KBr and placed into an in situ IR cell with CaF_2 windows. After alignment, the sample compartment was subjected to a thermal pretreatment in He flow at 250 °C for 2 h to remove the moisture. The sample cell was cooled to room temperature and switched to pure CO flow (99.5%) for 0.5 h. The absorption spectra were recorded at room temperature (4000–900 cm^{-1}, resolution of 1 cm^{-1}, and scan for 1 min). X-ray photoelectron spectroscopy (XPS) was measured on a VG Escalab 250 spectrometer equipped with an Al anode (Al Kα = 1846.6 eV). The background pressure in the analysis chamber was lower than 1×10^{-7} Pa. Measurements were performed using 20 eV pass energy, 0.1 eV step, and 0.15 dwelling time. Energy correction was carried out using the C1s peak of adventitious C at 284.6 eV.

2.4. Catalytic reaction

The solvent-free aerobic oxidation of benzyl alcohol using molecular O_2 was carried out in a bath-type reactor operated under atmospheric conditions: a three-necked glass flask (capacity: 25 mL) precharged with certain amount of reactant and catalyst as well as a stirring bar was heated in a silicon oil bath, where a thermocouple was applied to control the reaction temperature. A reflux condenser was employed to condense the hot vapor of products. The amount of reactant and catalyst was constant at alcohol/Pd = 250 mol/g. In each reaction run, the mixture was heated to the desired reaction temperature under vigorous stirring (stirring rate: 1200 rpm). Oxygen flow was bubbled at certain flow rate controlled by a mass flow controller into the mixture to initiate the reaction. After the allowed reaction time duration, the catalyst powder was filtered off, and the liquid organic products were analyzed using an Agilent gas chromatograph 6890 equipped with a HP-5 capillary column. Dodecane was the internal standard to calculate benzyl alcohol conversion and benzaldehyde selectivity. The conversion of benzyl alcohol and the selectivity toward benzaldehyde and quasi-turnover frequency (qTOF) are defined as follows:

$$\text{conversion } (\%) = 100\% \times \frac{\text{moles of reactant converted}}{\text{moles of reactant in feed}}$$

$$\text{selectivity } (\%) = 100\% \times \frac{\text{moles of product formed}}{\text{moles of reactant converted}}$$

$$\text{qTOF } (h^{-1}) = \frac{\text{moles of reactant converted}}{\text{moles of total active sites} \times \text{reaction time}}$$

3. Results

3.1. Effect of functional groups

The bulk average information of TUD-1 mesoporous silica and the effect of surface functionalization with various organosilanes were assessed by N_2 physisorption. The amount of different organosilanes was kept as 1.2 mmol/g TUD-1. The nitrogen adsorption–desorption isotherms and the corresponding pore size distributions are illustrated in Fig. 1a. The plots are typical type IV isotherms with a pronounced H3 hysteresis loop characteristic for mesostructured feature with a large pore diameter. Siliceous TUD-1 shows a sharp step increase at P/P_0 = 0.6–0.8 due to the capillary condensation of N_2 inside the mesopores. The step increase shifts to lower P/P_0, particularly for ATMS-TUD, suggesting a smaller pore size after surface functionalization with organosilanes, which can be directly observed from the pore size distributions in the inset of Fig. 1a. A summary of surface area, pore volume, and pore diameter is listed in Table 1 (entry 1–4, 7). Pristine TUD-1 exhibits a BET surface area of 529 $m^2\ g^{-1}$, pore volume of 0.99 $cm^3\ g^{-1}$, and a narrow pore size distribution centered at 7.5 nm, which are in good agreement with the previous report [18]. Surface functionalization results in an apparent decrease in these textural parameters, which can be attributed to the immobilization of organic functional groups on the inner wall of

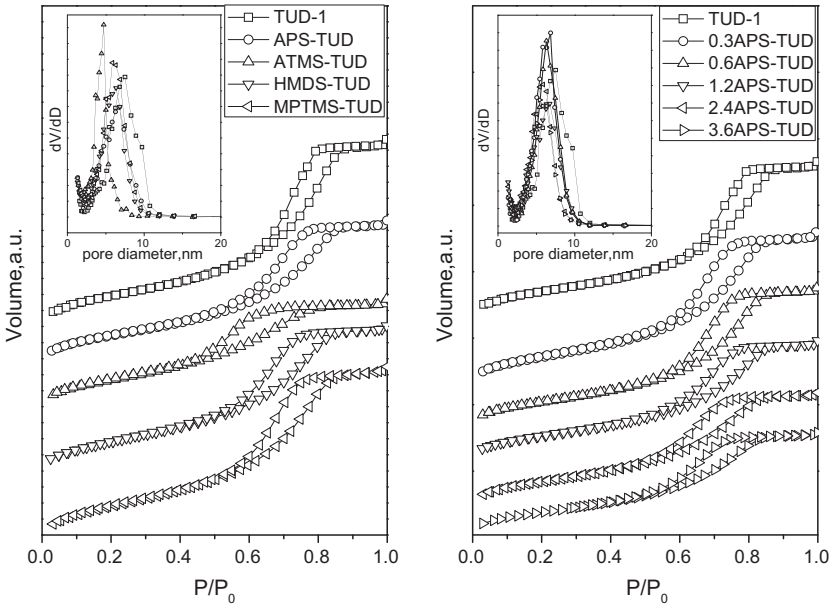

Fig. 1. (a) N_2 physisorption isotherms and inset pore size distribution of pristine and surface-functionalized TUD-1; (b) N_2 physisorption isotherms and inset pore size distribution of TUD-1 surface functionalized with different APS contents.

Table 1
Textural properties of pristine and surface-functionalized TUD-1 supports.

Entry	Sample	pH	Surface area ($m^2\ g^{-1}$)	Pore volume ($cm^3\ g^{-1}$)	Pore diameter (nm)
1	TUD-1	6.3	529	0.99	7.5
2	ATMS-TUD	9.7	396	0.62	4.7
3	HMDS-TUD	7.4	403	0.74	6.3
4	MPTMS-TUD	4.8	394	0.72	6.0
5	0.3APS-TUD	7.8	515	0.99	6.8
6	0.6APS-TUD	8.2	502	0.88	6.3
7	1.2APS-TUD	9.1	420	0.79	6.8
8	2.4APS-TUD	9.1	416	0.76	5.9
9	3.6APS-TUD	9.2	362	0.64	5.5

mesopores. It is worth mentioning that APS-TUD exhibits a decrease of 0.7 nm in pore diameter. Considering the organic group dimension (ca. 0.6 nm) and assuming these groups adopt a folded conformation [24], this diameter decrease can be suggested as a monolayer of aminopropyl groups covering the inner wall of mesopores. ATMS possesses diamine groups with the longest chain, resulting in a more extended conformation structure; ATMS-TUD shows the most significant variation in pore volume and pore diameter, which is consistent with the lowest onset condensation step in the N_2 physisorption isotherms. As mentioned earlier, the average pH of support surface, which reflects the surface chemistry to certain extent, plays a crucial role in the selective oxidation of benzyl alcohol. The results of pH measurement of pristine and surface-modified TUD-1 supports are also summarized in Table 1. It is noteworthy that the pH varies significantly with surface functionalizations. The surface of pristine TUD-1 is mildly acidic, showing a pH of 6.3. Surface functionalization with both APS and ATMS increases the pH to 9.1 and 9.7, respectively, showing that silylation with amino groups provides the effective raise in the surface basicity of silica support. HMDS-functionalization exhibits a neutral surface as expected. Silylation with MPTMS notably reduces the pH to 4.8 due to the presence of thiol group. All these changes in pH validate the successful surface functionalizations and the effectively tuned surface basicity of TUD-1 support.

Fig. 2 displays the FTIR spectra of pristine and surface-functionalized TUD-1. All TUD-1 samples, regardless of surface functionalization, show typical bands at 1090 and 798 cm^{-1} in the skeletal region of framework vibrations, which are assigned to the asymmetric and symmetric stretching vibrations of Si–O–Si bridges, respectively [25]. The absorbance at 1090 cm^{-1} has a slight blue shift after surface functionalization, which can be attributed to the shrinkage of pore structure [26]. The absorbance at 965 cm^{-1}

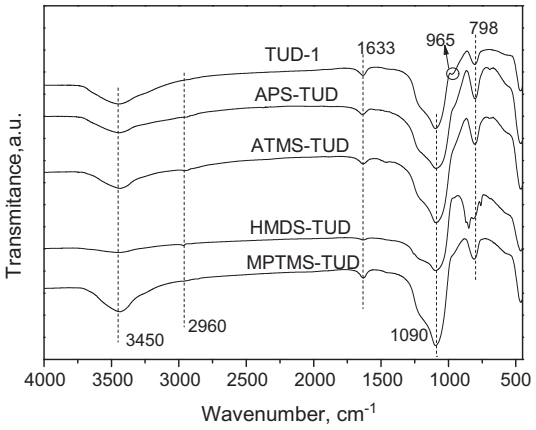

Fig. 2. FTIR spectra of pristine and surface-functionalized TUD-1 with different modifiers.

for pristine TUD-1 assignable to the stretching vibrations of terminal silanol (Si–OH) groups disappears upon the surface modification [25], implying the successful replacement of terminal silanol groups with organosilane modifiers. Luan et al. suggested that these abundant silanol groups on the inner surface of mesopores serve as the sites for grafting functional groups during the surface modification [27]. In the hydroxyl region, the weak band at 1633 cm^{-1} and the broad band at 3450 cm^{-1} can be attributed to a combination of the stretching vibration of silanol groups or silanol "nests" with cross hydrogen-bonding interactions and the H–O–H stretching mode of physisorbed water [27]. The absence of these two bands for HMDS-TUD suggests the successful silylation of isolated silanol groups with HMDS, leading to the formation of a hydrophobic surface due to $Si(CH_3)_3$ groups. The presence of a broad inconspicuous band at 2960 cm^{-1}, which is characteristic of the asymmetric vibration of the CH_2 groups of silylating agents, further confirms the successful silylation [28].

XRD and TEM characterization techniques were introduced to examine the Pd catalysts supported on these surface-functionalized TUD-1 silicas. The XRD patterns of 1 wt.% Pd-containing catalysts are shown in the Supporting information Fig. S1. No distinct diffraction peak can be observed except for 1Pd/TUD and 1Pd/HMDS-TUD, implying the highly dispersed nature of these metallic nanoparticles. For 1Pd/TUD and 1Pd/HMDS-TUD, a diffraction peak indexed to the (1 1 1) facet of face-centered cubic (FCC) lattice structure of Pd metal is discernable, suggesting the formation of metallic Pd nanocrystals with a relatively larger particle size for these two samples. These XRD analyses can be further confirmed by the direct TEM microscopic observation. The TEM images and the corresponding particle size distributions derived from counting ca. 300 particles are illustrated in Fig. 3. TUD-1 shows a sponge-like porous structure, suggesting the successful synthesis of TUD-1 mesostructure and good stability after metal adsorption and reduction. In agreement with nitrogen physisorption results, the lack of long-range ordered mesostructure in TUD-1 after metal adsorption and reduction is also reflected in the TEM image. 1Pd/TUD exhibits a broad palladium particle size distribution centered at 7.0 nm, which is consistent with the pore diameter of pristine TUD-1 (7.5 nm), implying the encapsulation of Pd nanoparticles in the mesopores of TUD-1. Upon surface functionalization, 1Pd/APS-TUD, 1Pd/ATMS-TUD, and 1Pd/MPTMS-TUD show narrow particle size distributions with mean particle diameters of 1.9, 3.2, and 1.6 nm, respectively. Nonetheless, 1Pd/HMDS-TUD exhibits a considerably wide particle size distribution with a mean particle size of 17.0 nm.

After surface functionalization via the silylation of TUD-1 silica matrix with various organosilanes, these immobilized functional groups bonded onto the inner pore wall surface of TUD-1 act as anchors for the metal adsorption. Hydrophilic amino groups ($-NH_2$) and thiol groups (–SH) show great affinity to the aqueous palladium chloride and therefore facilitate the deposition of metal precursor and the formation of small and highly dispersed Pd nanoparticles embedded on TUD-1. Furthermore, 1Pd/HMDS-TUD with hydrophobic trimethyl groups shows a barrier for the adsorption of Pd precursor and leads to the formation of large Pd particles with board particle diameter distribution. 1Pd/APS-TUD displays a narrower Pd particle size distribution and a smaller mean particle diameter than 1Pd/ATMS-TUD (see Fig. 3b and c). Lee et al. also reported a similar result, and they attributed it to the strong interaction between Pd nanoparticles and the grafted diamino groups [29]. The substantially small pore diameter and pore volume of 1Pd/ATMS-TUD may also play a role in forming the Pd nanoparticles with an irregular size distribution, which has been indicated in our previous report [15].

We introduced the solvent-free selective oxidation of benzyl alcohol using molecular oxygen as a model reaction to examine

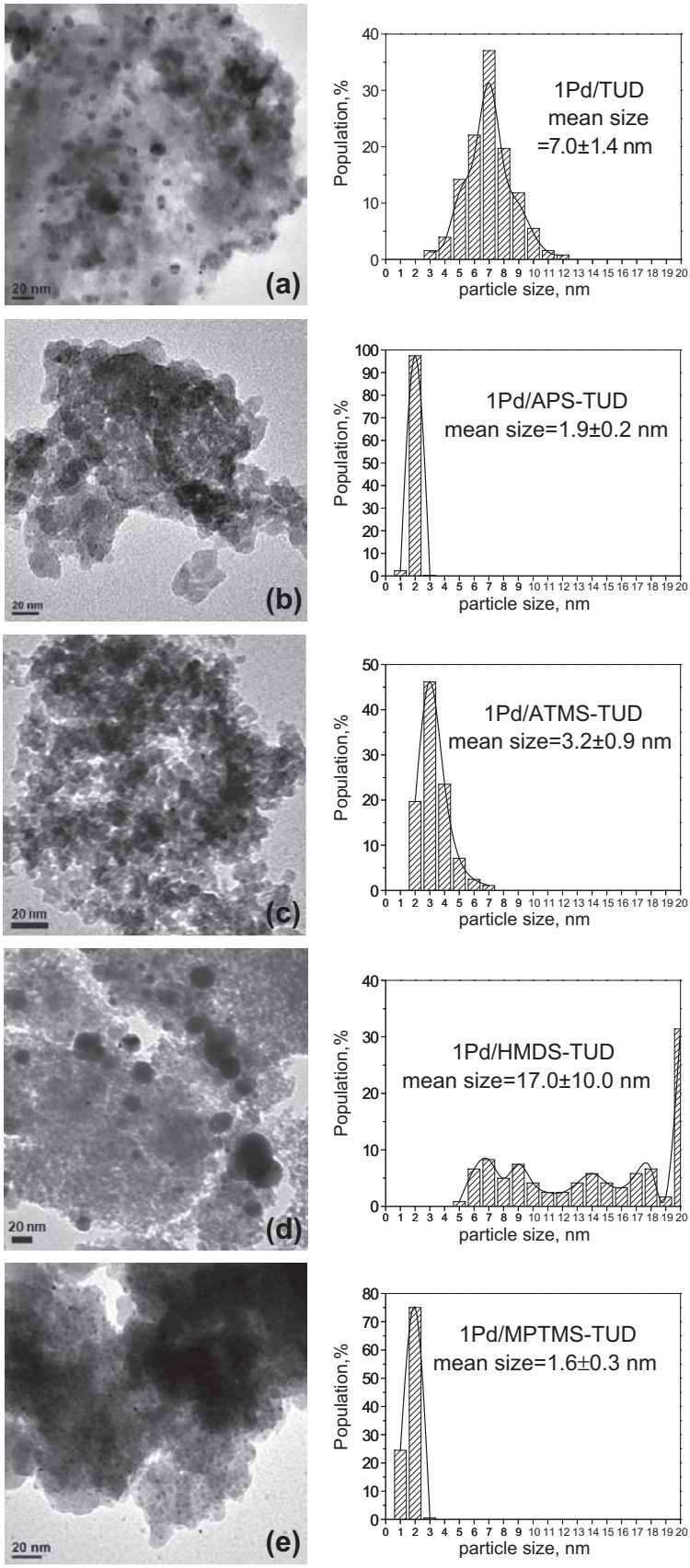

Fig. 3. TEM micrographs and particles size distributions of 1 wt.% Pd supported on TUD-1 surface functionalized with different modifiers: (a) 1Pd/TUD; (b) 1Pd/1.2APS-TUD; (c) 1Pd/ATMS-TUD; (d) 1Pd/HMDS-TUD; (e) 1Pd/MPTMS-TUD.

Table 2
Catalytic properties of Pd-containing catalysts supported on pristine and surface-functionalized TUD-1.[a]

Catalyst	Pd content[b] (wt.%)	Conversion (%)	Selectivity (%)			qTOF[c] (h^{-1})
			Benzaldehyde	Toluene	Benzoic acid	
1Pd/TUD	0.68	13.2	91.7	1.5	6.8	12,910
1Pd/APS-TUD	0.99	22.3	95.2	0	4.8	18,571
1Pd/ATMS-TUD	0.97	17.0	93.5	0	6.5	13,179
1Pd/HMDS-TUD	0.41	11.5	91.5	0	8.5	16,802
1Pd/MPTMS-TUD	0.77	26.3	81.5	17.7	0.8	29,456

[a] Reaction conditions: benzyl alcohol/Pd = 250 mol/g; O_2, 20 mL min^{-1}; temperature, 160 °C; reaction time, 1 h; stirring rate, 1200 rpm.
[b] Pd content was tested by ICP.
[c] qTOF is calculated by using the Pd content obtained from ICP and subtracting the non-catalytic effect (conversion ~5%)

these as-synthesized Pd catalysts, aiming to elucidate the effect of surface functionalization on catalytic performance. The catalytic results are listed in Table 2, where qTOF was determined by using the Pd content obtained from ICP tests and subtracting the non-catalytic effect (benzyl alcohol conversion of ~5% at 160 °C). Benzaldehyde is produced as the main product along with a trace amount of toluene and benzoic acid as by-products. The catalytic activity is remarkably enhanced upon the surface functionalization after we rule out the effect of actual metal loadings. Among all the catalysts, 1Pd/MPTMS-TUD shows the best catalytic activity with a conversion of 26.3% and an exceptionally high qTOF of 29,456 h^{-1}, which is twice that of 1Pd/TUD. Nevertheless, this high activity is accompanied by the formation of a large amount of toluene and benzoic acid, resulting in consequently low benzaldehyde selectivity (81.5%). No toluene was detected for other surface-modified catalysts, and benzoic acid is the only by-product.

Recalling the TEM results in Fig. 3, uniform Pd nanoparticles with a narrow size distribution centered at 1.6 nm on 1Pd/MPTMS-TUD explain the remarkably high activity of this particular catalyst, implying that the Pd nanoparticle size plays a vital role in controlling the catalytic activity, which is coincident with the results reported by Li et al. [4]. Nevertheless, the catalytic activity of noble metal catalysts in the selective oxidation of alcohols heavily relies on the metal–support interaction in addition to the mean metal particle size. Over 1Pd/MPTMS-TUD, a large amount of toluene as by-product is induced by the acidic surface due to the hydrolysis of –SH groups, as suggested by Enache et al. [30]. Furthermore, the generation of benzoic acid is suppressed, and thus the improvement in benzyl alcohol conversion over 1Pd/MPTMS-TUD is mainly attributed to the formation of toluene by disproportionation of benzyl alcohols. The extremely low Pd content in 1Pd/HMDS-TUD is due to the adsorption barrier of aqueous palladium precursor onto the hydrophobic surface in the presence of trimethyl groups. This particular catalyst exhibits the lowest benzyl alcohol conversion (11.5%), which probably resulted from the lack of active sites due to the extremely low Pd content as well as the large and irregular Pd nanoparticles as indicated in XRD and TEM.

For amino group-functionalized catalysts, i.e., both 1Pd/APS-TUD and 1Pd/ATMS-TUD, the surface is basic due to the hydrolysis of amino groups, which slightly promotes the formation of benzoic acid. The elevated surface basicity is suggested to enhance the dehydrogenation of benzyl alcohol, which is the rate-controlling step during the reaction, suppress the formation of by-product toluene, as well as facilitate the reactant adsorption and product desorption from the Pd active sites. Although APS and ATMS both contain amino groups, 1Pd/APS-TUD exhibits larger enhancement in the catalytic activity as well as the selectivity. This is mainly due to the formation of larger Pd nanoparticles with fewer active sites for the reaction in 1Pd/ATMS-TUD as suggested by TEM because diamine groups in ATMS show stronger interaction with Pd nanoparticles than that of monoamine groups in APS. After considering both excellent catalytic activity and high selectivity toward benzaldehyde, APS was selected as the best modifier in the following study.

3.2. Effect of APS amount

The nitrogen physisorption patterns of TUD-1 surface functionalized with different APS contents varying from 0.3 to 3.6 mmol/g TUD-1, as shown in Fig. 1b, exhibit irreversible type IV isotherms, which are identical to that of pristine TUD-1. Increasing the APS loading amount notably shifts the hysteresis toward a lower relative pressure (P/P_0) and slightly decreases the overall nitrogen adsorption volume, implying the successful grafting of APS on the inner wall of TUD-1 mesopores. The narrow pore size distributions are shown in the inset of Fig. 1b. The calculated textural parameters of TUD-1 modified with various APS amounts are listed in Table 1 (entry 1, 5–9). The APS-modified TUD-1 samples show comparable structural parameters to the parent TUD-1, implying that the integrity of pristine mesoporous structure is retained after the surface-grafting procedure. A trend of decreasing surface area, pore volume, and pore diameter with increasing APS content can be observed, which is attributed to the self-assembly and incorporation of functional groups into the framework of mesoporous materials. The results of pH measurement of TUD-1 supports surface functionalized with different APS amounts are also listed in Table 1. Increasing the APS amount notably increases the pH level from 6.3 for pristine TUD-1 to 9.1 for 1.2APS-TUD, indicating that the local surface basicity can be remarkably elevated after silylation with an appropriate amount of APS. However, further increasing the APS content does not substantially increase the pH value, which is probably due to that a maximum grafting amount of APS exists as suggested by Ramila et al. [31].

According to Xu et al., well-isolated amino group and hydroxyl group absorption bands cannot be resolved using FTIR because of the bending vibration overlap between N–H and hydroxyl or silanol groups in IR range [32]. Near-infrared (NIR) is superior to IR for characterizing amino groups because amino groups exhibit well-resolved absorption bands in the NIR region (1000–2500 nm). As illustrated in Fig. 4a. All the APS-modified TUD-1 samples display two major absorption bands: 1897 nm assignable to the combination of stretching and deformation vibrations for adsorbed water and 1403 nm ascribable to the first overtone of the stretching frequencies of silanol groups and adsorbed water [33]. Upon grafting APS onto TUD-1 surface, the reflection bands at 1528 and 2020 nm appear and become more and more intense as increasing the APS loading amount. These two bands are indexed to the combination band of asymmetry stretching (ν_{asym}) and symmetry stretching (ν_{sym}) modes and the combination band of stretching vibration (ν) and bending (δ) modes of the amino groups, respectively [34]. Moreover, the reflection bands between 1600 and 860 nm are assigned to the stretching vibration of CH_2 moiety in the propyl chain of the APS silane modifier [35]. The UV–vis–NIR spectra provide further evidence that after surface

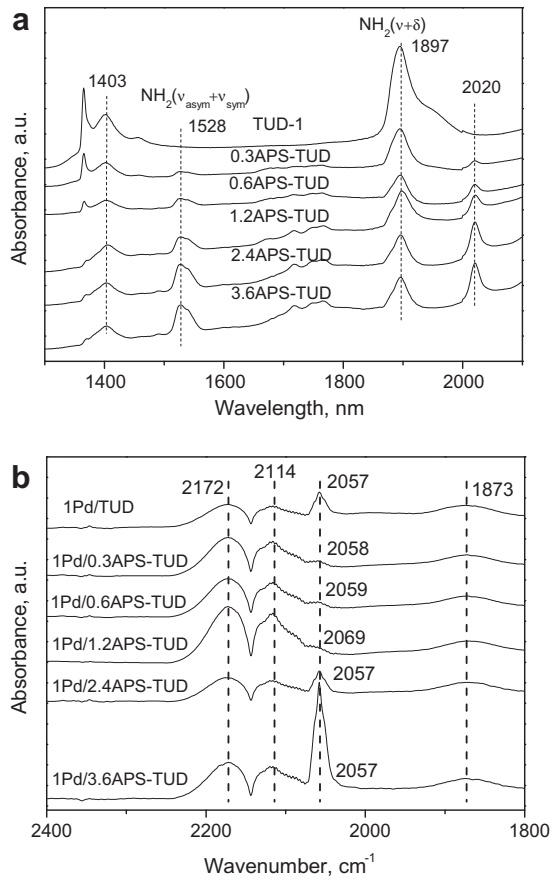

Fig. 4. (a) The UV–vis–NIR spectra of pristine and APS-functionalized TUD-1 with different APS contents; (b) IRA spectra for CO adsorption on 1Pd/APS-TUD with different APS contents. CO dosage and measurement performed at room temperature.

modification with APS, the amino functional groups are indeed grafted onto the silica surface and covalently bonded to the inner wall of mesopores.

Vibrational spectroscopy techniques, e.g., IRAS, have been regarded as exceptionally useful tools for elucidating the heterogeneous catalytic reaction mechanisms, indentifying the active species on a catalyst surface with sub-monolayer accuracy, and addressing the particle size and morphology effects and particle–support interactions. In this study, IRAS was employed using CO as a probe molecule to identify specific interaction between Pd nanoparticles and amino groups. All samples show the characteristic features for CO adsorption on Pd nanoparticles, see Fig. 4b. The bands at 2172 and 2114 cm^{-1} are assigned to the absorption of residual gaseous CO. These two characteristic bands do not change significantly with increasing the APS amount. The C–O stretching bands at around 2057 and 1873 cm^{-1} correspond to the CO molecules adsorbed on top and threefold hollow sites on a (1 1 1) facet of Pd nanoclusters, respectively, suggesting that TUD-1-supported Pd nanoparticles in this study exhibit predominantly (1 1 1) facets, which in agreement with previous reports [36].

With increasing grafted amount of aminopropyl groups, the absorption band at 2057 cm^{-1} becomes boarder and slightly blue shifts to high wave number. In particular, this band shifts to 2069 cm^{-1} and becomes an imperceptible shoulder for 1Pd/1.2APS-TUD. When the APS contents further increase, this band becomes narrower and shifts back to 2057 cm^{-1} as that of Pd supported on pristine TUD-1. The information of Pd nanoparticle size and interaction between Pd and amino groups can be indirectly derived from this variation of absorption bands. The decreased Pd nanoparticle size can lead to the broadening and blue shift of CO stretching band in IRA spectra, which is due to the increased number of defect sites (such as edges and kinks) and disorder on a small Pd nanoparticle, as suggested by Ozensoy and Goodman [36]. Hollins reported that the increase in CO stretching frequency is also attributed to a weaker CO–metal interaction, resulting in a reduced occupation of CO 2π orbital when CO is bound at a high-coordinated metal atom [37]. With increased grafting content of aminopropyl groups, Pd atoms have higher coordination with the surrounding amino groups; the interaction between Pd nanoparticles and the APS-modified TUD-1 becomes stronger. Hence, the interaction between Pd and adsorbed CO gets weaker and less CO 2π orbit is occupied, leading to the blue shift of the CO stretching band.

To further investigate the structural and electronic properties of these Pd nanoclusters, Pd 3*d* XPS measurements were conducted, and the results of four selected 1Pd/APS-TUD samples are illustrated in Fig. 5. All the samples show a typical doublet of 3*d* core level bands centered around 340 and 335 eV, which are assigned to Pd^0 $3d_{3/2}$ and Pd^0 $3d_{5/2}$, respectively [38]. Recently, Radkevich et al. have demonstrated the amino groups possessing electron-donor properties can increase the proportion of Pd^0 and the resistance against re-oxidation of Pd^0 due to the electronic interactions between nitrogen atoms and Pd metallic nanoparticles, which are active centers for hydrogenation–dehydrogenation reactions [39]. We cannot draw the same conclusion because no oxide peak is detected throughout the whole Pd 3*d* region, implying the formation of Pd metallic nanoparticles by completely reducing the palladium precursors. With increasing grafted amount of APS, both bands undergo a negative shift to lower binding energies. The maximum shift (1 eV) when compared to the binding energy of Pd supported on pristine TUD-1 can be observed on 1Pd/1.2APS-TUD. With

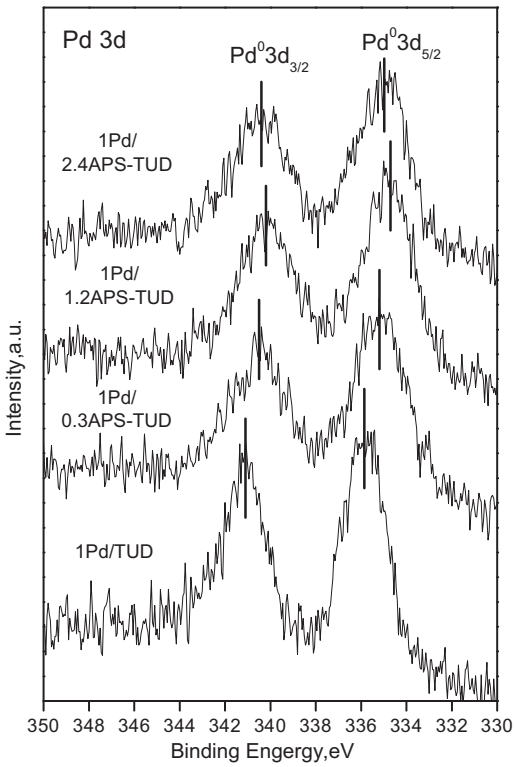

Fig. 5. TEM micrographs and particles size distributions of 1Pd/APS-TUD with different APS contents: (a) 1Pd/0.3APS-TUD; (b) 1Pd/0.6APS-TUD; (c) 1Pd/1.2APS-TUD; (d) 1Pd/2.4APS-TUD; (e) 1Pd/3.6APS-TUD.

further increase in the APS content, both bands exhibit a shift back to high binding energy. Fox et al. suggested that the shift to low binding energy indicates the high dispersion of Pd species [40]. It is worthwhile noticing that this trend of binding energy shift is

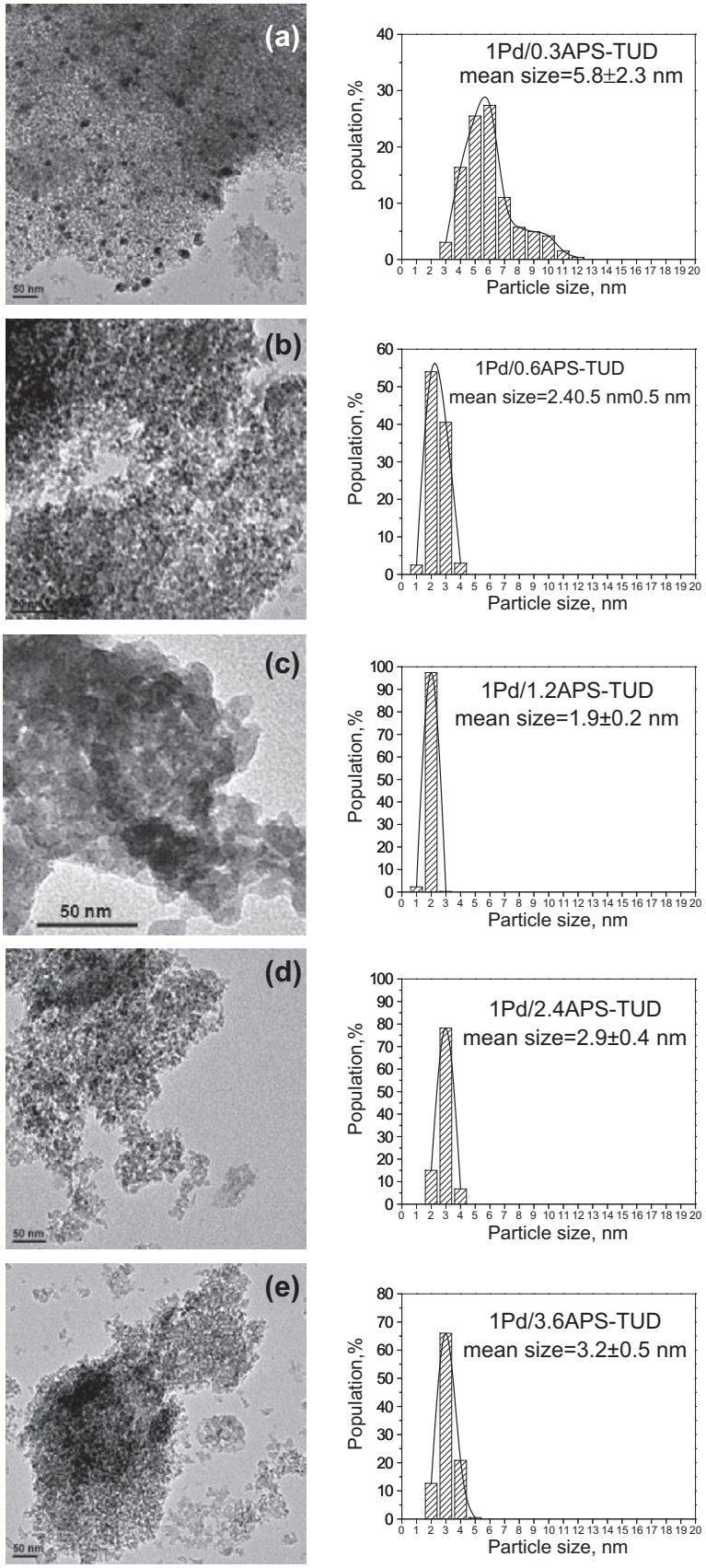

Fig. 6. Pd 3d XP spectra of 1Pd/APS-TUD catalysts with various APS contents.

identical to that of CO adsorption peak from IRAS and can be understood as complementary evidence of the APS amount effect on the interaction between Pd nanoparticles and amino groups.

The XRD patterns of 1Pd/APS-TUD catalysts with different APS amounts are shown in the Supporting information Fig. S2. There is no obvious discrepancy in the Pd nanoparticles dispersion among all 1Pd/APS-TUD catalysts because no noticeable diffraction peak can be observed in the XRD patterns. The TEM images are shown in Fig. 6. The mean Pd particle size is reduced from 7.0 to 5.8 nm upon increasing surface modification with APS. It decreases to 1.9 nm with a narrow size distribution for 1Pd/1.2APS-TUD. Nevertheless, larger Pd nanoclusters are formed with a boarder particle size distribution for 1Pd/3.6APS-TUD due to the excess amount of APS. This trend is consistent with IRAS and XPS results. It can be verified that the grafting amount of amino groups plays an important role in controlling the size and morphology of Pd nanoparticles, i.e., small and homogeneous Pd nanoparticles formed upon surface functionalized with APS, whereas further loading excess APS results in large and irregular nanoparticles. A specific interaction between Pd nanoclusters and APS immobilized TUD-1 support is also evidenced.

Romanmartinez et al. suggested that the distribution of metal precursors on the support and the specific metal–support interaction are strongly dependent on the support surface chemistry [41]. This APS effect on the size control of Pd nanoparticles can be explained by the nature of the support surface, which results in different interactions between metal and support. Due to the hydrolysis in the metal adsorption procedure, the silica surface without APS group is mildly acidic and negatively charged, which hinders the diffusion and adsorption of negatively charged $PdCl_2(OH_2)^{2-}$ species. After substituting the terminal silanol groups with amino groups, the surface is positively charged due to the hydrolysis of $-NH_2$ groups, exhibiting great affinity to the palladium precursors, thus the palladium precursors can be easily adsorbed into the mesopores. In addition, these immobilized amino groups are suggested to act as anchors to stabilize the Pd nanoparticles by binding them through covalent interactions, resulting in highly dispersed and uniformly distributed Pd nanoparticles [11]. Nevertheless, further adding APS may result in the oligomerization and polymerization of organosilanes into the form of a cross-linked monolayer of alkanolamine attached on the surface; partially, blocking the mesopores occurs as suggested in nitrogen physisorption (see Table 1) [42]. More Pd nanoparticles on the external surface of the support are susceptible to agglomeration due to the lack of structural confinement [15]. Thus, there is a optimized amount of APS functional groups to substitute the silanol groups and occupy the pore volume, which was also demonstrated by other groups [27,31]. In this study, the effect of APS content is pronounced between 1.2APS-TUD substrate and Pd species.

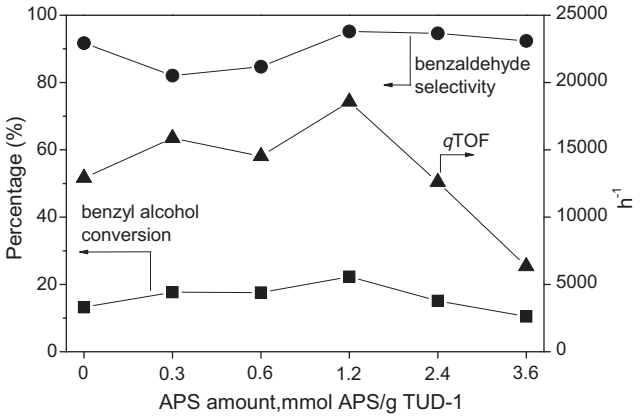

Fig. 7. Catalytic performance of 1Pd/APS-TUD catalysts with different APS contents. Reaction conditions: benzyl alcohol/Pd = 250 mol/g; O_2, 20 mL min^{-1}; temperature, 160 °C; reaction time, 1 h; stirring rate, 1200 rpm.

To examine the effect of grafted APS content on the catalytic activity, benzyl alcohol oxidation over 1Pd/APS-TUD catalysts with different APS amounts was investigated and illustrated in Fig. 7. The catalytic activity is improved when APS is grafted. 1Pd/1.2APS-TUD shows the highest conversion and selectivity toward benzaldehyde of 22.3% and 95.2%, respectively. Further increasing the APS loading slightly decreases the catalytic activity and selectivity. The trend of benzyl alcohol conversion implies the activity of supported Pd catalysts is mainly dependent on the particle size and size distribution [4] as well as the local surface basicity. The outstanding catalytic behavior of 1Pd/1.2APS-TUD resulted from the small and uniform Pd nanoparticles due to the enhanced metal–support interaction and the appropriate surface basicity. 1Pd/1.2APS-TUD was selected as the optimal catalyst in the following work.

3.3. Effect of Pd loading

The XRD patterns of Pd/1.2APS-TUD with different Pd loadings (0.5–3 wt.%) illustrate that only 3Pd/1.2APS-TUD shows a weak and broad diffraction peak assigned to the (1 1 1) facet of face-centered cubic (FCC) lattice structure for Pd nanoparticles, suggesting the formation of large and irregular Pd nanoclusters in this particular sample. It is further demonstrated by the direct TEM microscopic images as displayed in Fig. 8. Increasing Pd loading results in a larger mean particle diameter, varied between 1.3 nm for 0.5Pd/1.2APS-TUD and 6.5 nm for 3Pd/1.2APS-TUD. Moreover, the nanoparticles on 3Pd/1.2APS-TUD show a wide size distribution. This discrepancy is mainly caused by the agglomeration of Pd nanoparticles due to high Pd content.

The catalytic results of benzyl alcohol oxidation over Pd/1.2APS-TUD catalysts with different Pd loadings are shown in Fig. 9. All catalysts exhibit a high and constant selectivity around 96% toward benzaldehyde. The benzyl alcohol conversion increases as the Pd loading rises from 0.5 to 1 wt.%, which is due to the increased number of active sites available participating in the reaction. The conversion slightly decreases upon further adding Pd, which can be attributed to the agglomeration of nanoparticles which decreases the available number of active sites for the reaction at a high Pd content [4]. Among all the samples, 1Pd/1.2APS-TUD shows the best catalytic result with a remarkably high qTOF of 18,571 h^{-1} and is regarded as the best catalyst in this study.

The inset table in Fig. 9 lists the activation energies of these catalysts in aerobic oxidation of benzyl alcohol determined from the Arrhenius plots. These activation energy values are comparable to that of TiO_2-supported noble metal catalysts reported by Enache et al. (45.8 kJ/mol) [30] and much higher than the Pd catalyst supported on SBA-16 (12.3 kJ/mol) [16]. It was reported that low activation energy in a liquid phase reaction indicates the alcohol oxidation is likely to be mass diffusion limited and controlled by the access of reactants to active sites [43]. This suggests that the unique 3-D sponge-like mesoporous structure of TUD-1 can effectively eliminate the diffusion limitation.

3.4. Studies on the 1Pd/1.2APS-TUD catalyst

1Pd/1.2APS-TUD, which has been verified possessing the best catalytic performance in the solvent-free oxidation of benzyl alcohol, was investigated in detail. The time course of 1Pd/1.2APS-TUD for benzyl alcohol oxidation was monitored periodically, as depicted in Fig. 10. Benzyl alcohol conversion monotonically increases with the reaction time duration along with a

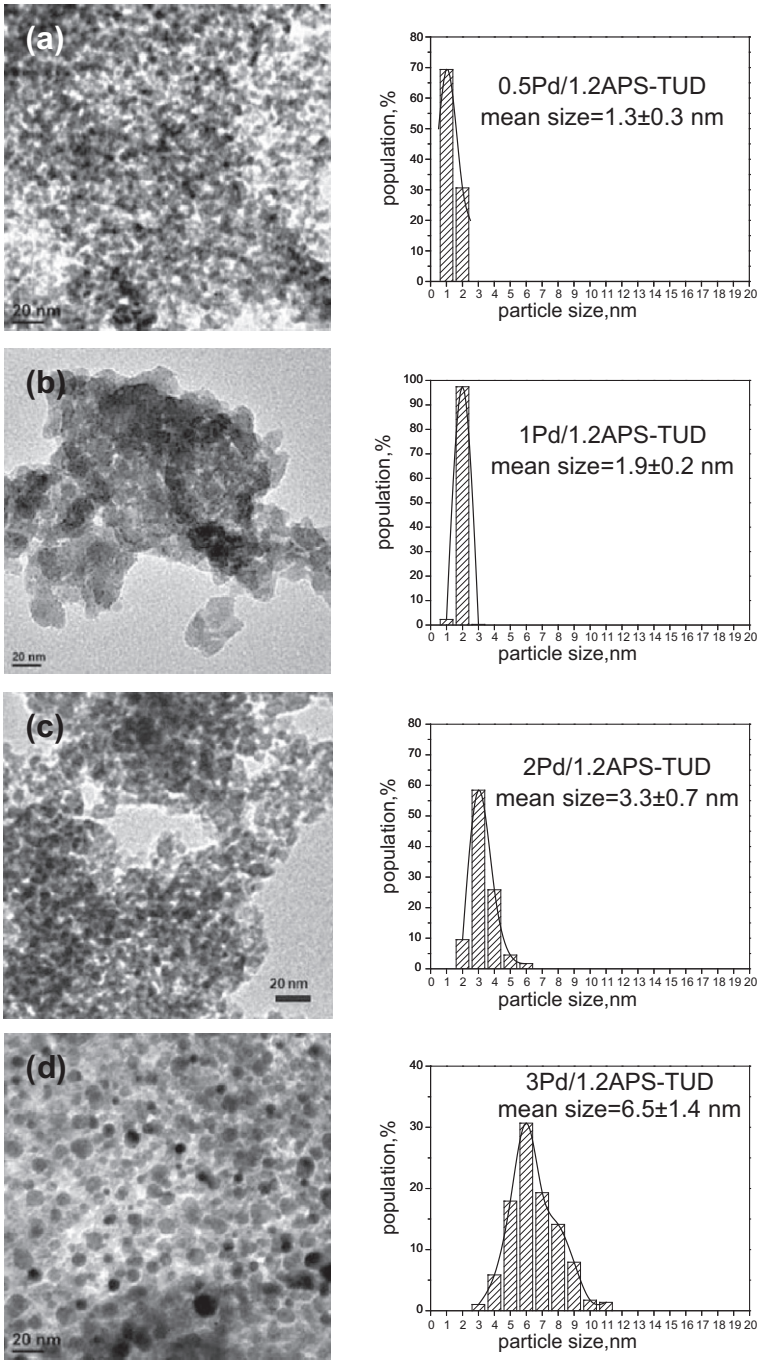

Fig. 8. TEM micrographs and particles size distributions of Pd/1.2APS-TUD with various Pd loading: (a) 0.5Pd/1.2APS-TUD; (b) 1Pd/1.2APS-TUD; (c) 2Pd/1.2APS-TUD; (d) 3Pd/1.2APS-TUD.

rapidly declined qTOF. The selectivity toward benzaldehyde is rather low (81.5%) at first 0.5 h of reaction; it rises to 95.2% at 1 h and gradually decreases afterward. The poor selectivity at first 0.5 h is contributed by the formation of a large amount of toluene (15.8%), which is produced from the hydrogenolysis of benzyl alcohol facilitated by hydrogen adsorbed on Pd surface formed in the dehydrogenation step at the beginning of reaction [44]. The decay of selectivity at long reaction time is ascribed to the generation of benzoic acid due to the further oxidation of benzaldehyde.

The effects of reaction temperature and oxygen flow rate were also examined and summarized in Table 3. Neither TUD-1 nor surface-functionalized TUD-1 displayed noticeable catalytic activity at a low reaction temperature. The selectivity toward benzaldehyde is well maintained above 95% when the temperature increases from 80 to 160 °C (entry 1–5). Benzyl alcohol conversion is extremely low at low reaction temperatures, and it remarkably increases when the temperature is elevated from 120 to 160 °C. The benzyl alcohol conversion displays a tenfold enhancement when the reaction temperature increases from 100 to 160 °C. This trend is consistent with the activation energies listed in Fig. 9. The high activation energy implies the absence of mass transport limitation, as well as the large energy barrier for the reaction. Therefore, high temperature is beneficial to initiate the reaction. The O_2 flow also shows impact on the catalytic performance. The selectivity to benzaldehyde is low accompanied by the formation of a large amount of toluene at low O_2 flow rate, and the selectivity gradually improves

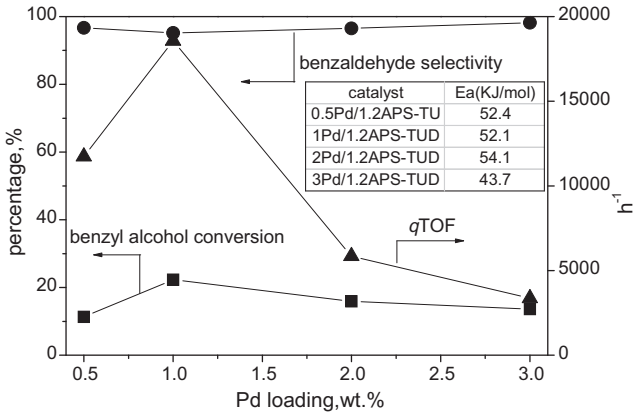

Fig. 9. Catalytic performance of Pd/1.2APS-TUD with various Pd loadings and inset table of activation energy. Reaction conditions: benzyl alcohol/Pd = 250 mol/g; O_2, 20 mL min^{-1}; temperature, 160 °C; reaction time, 1 h; stirring rate, 1200 rpm.

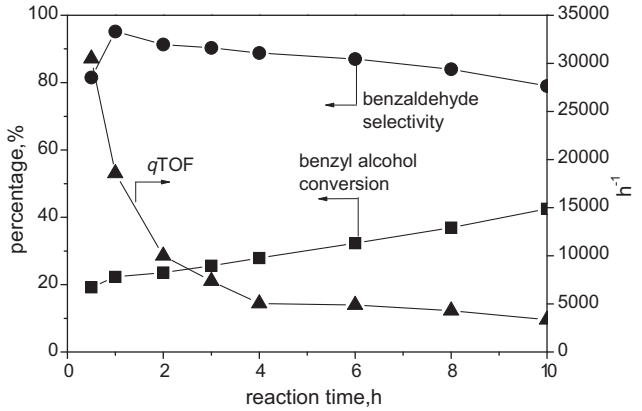

Fig. 10. Time course of 1Pd/1.2APS-TUD for benzyl alcohol oxidation. Reaction conditions: benzyl alcohol/Pd = 250 mol/g; O_2, 20 mL min^{-1}; temperature, 160 °C; stirring rate, 1200 rpm.

with the increased flow rate (entry 5–7). Toluene has been verified as the major by-product under anaerobic conditions due to the deficiency of surface oxygen, which therefore results in either a concentrated nucleophilic attack of s surface hydride to the benzylic carbon of adsorbed benzyl alcohol or the recombination of [$PhCH_2$(ad)] with [H(ad)] [45]. Moreover, the slight decrease in conversion at a low O_2 flow rate also implies the possible presence of external diffusion effect, which can be eliminated by increasing the O_2 flow rate.

Several other aromatic alcohols were employed to examine the generality of 1Pd/1.2APS-TUD for alcohol oxidation, and the results are listed in Table 3 (entry 8–12). The selectivity toward the corresponding aldehyde or ketone is remarkably high for all the alcohols tested. High efficiency (qTOF of 29,576 h^{-1}) was obtained for 1-phenylethanol oxidation, implying the higher reactivity of secondary alcohol compared to primary alcohol. 4-methylbenzyl alcohol shows a low conversion but non-ignorable. Poor activities are observed for the oxidation of 4-nitrobenzyl alcohol and 4-bromobenzyl alcohol, suggesting that this 1Pd/1.2APS-TUD catalyst shows higher catalytic activity for substituted aromatic alcohols containing electron-donating group (e.g., $-CH_3$) than those containing electro-withdrawing groups (such as $-NO_2$ and –Br) [46]. Additionally, this catalyst also displays a good conversion for the oxidation of cinnamyl alcohol (entry 12), suggesting the effective catalytic activity for oxidizing allylic alcohols.

The recyclability has been taken as a curial factor in evaluating a heterogeneous catalyst participating in a multiphase system. The metallic components with weak stability and poor recyclability can leach out during the course of reaction, resulting in the formation of an active homogeneous catalyst and a loss of catalytic activity on subsequent consecutive runs. The recyclability of 1Pd/1.2APS-TUD catalyst in the solvent-free selective oxidation of benzyl alcohol with molecular oxygen was examined. The catalyst

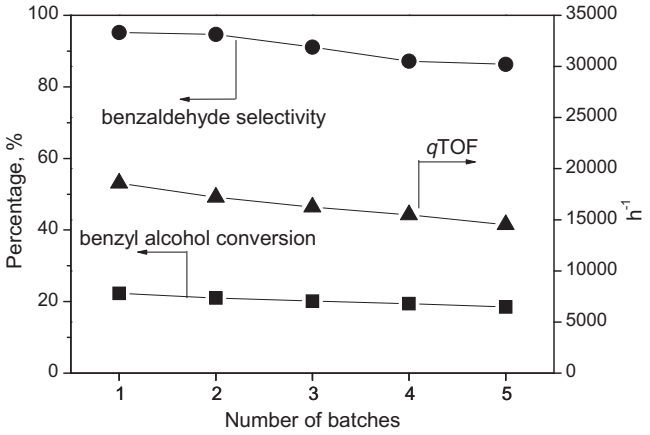

Fig. 11. Recyclability of 1Pd/1.2APS-TUD catalyst for solvent-free oxidation of benzyl alcohol with molecular oxygen. Reaction conditions: benzyl alcohol/Pd = 250 mol/g; O_2, 20 mL min^{-1}; temperature, 160 °C; reaction time, 1 h; stirring rate, 1200 rpm.

Table 3
Effect of reaction conditions for 1Pd/1.2APS-TUD on alcohol oxidation.[a]

Entry	Substrate	Temperature (°C)	O_2 flow rate (mL min^{-1})	Conversion (%)	Selectivity[b] (%)	qTOF (h^{-1})
1	Benzyl alcohol	80	20	0.8	96.2	908
2	Benzyl alcohol	100	20	2.2	96.6	2316
3	Benzyl alcohol	120	20	3.0	96.2	3251
4	Benzyl alcohol	140	20	10.7	94.5	11,493
5	Benzyl alcohol	160	20	22.3	95.2	18,571
6	Benzyl alcohol	160	10	18.8	83.7	14,847
7	Benzyl alcohol	160	5	14.4	79.9	13,329
8	1-Phenylethanol	160	20	27.5	98.2	29,576
9	4-Methylbenzyl alcohol	160	20	6.0	97.2	6437
10	4-Nitrobenzyl alcohol	160	20	1.0	100	1025
11	4-Bromobenzyl alcohol	160	20	0.8	100	874
12	Cinnamyl alcohol	160	20	14.4	100	15,493

[a] Reaction conditions: substrate/Pd = 250 mol/g; reaction time, 1 h; stirring rate, 1200 rpm.
[b] Selectivity refers to the corresponding aldehyde or ketone; for benzyl alcohol, by-products are toluene and benzoic acid; for 1-phenylethanol, by-product is ethylbenzene; for 4-methylbenzyl alcohol, by-product is *p*-xylene.

was recovered after each reaction run, washed with acetone, dried at 60 °C, and reused in a new reaction. Fig. 11 shows the recyclability of 1Pd/1.2APS-TUD for 5 consecutive cycles. The catalytic activity and selectivity only undergo a moderate decrease, which is attributed to the loss of catalyst during recovery. The Pd content after 5 consecutive reaction cycles was almost the same as that of fresh catalyst, and Pd cannot be detected by ICP analysis in the filtrate after the reaction. Moreover, no noticeable conversion of benzyl alcohol was observed when the liquid filtrate was employed instead of the solid catalyst for further reaction, further confirming that there was no leaching of Pd. Therefore, APS-modified TUD-1-supported Pd catalysts not only dramatically improve the catalytic performance but also show superiority in enhancing the resistance against deactivation.

4. Discussion

To demonstrate the advantage of TUD-1's unique mesostructure in the liquid phase reaction, we investigated the catalytic performances of Pd catalysts supported on various surface-functionalized mesoporous silica materials, including TUD-1, MCM-41 and SBA-15 with 2-D hexagonal structure and SBA-16 with 3-D cubic cage-like structure. As depicted in Fig. 12, TUD-1 shows superior catalytic activity relative to other silica materials, regardless of the surface functionalization. SBA-16 shows a moderate performance, whereas MCM-41 and SBA-15 exhibit a similar but rather low activity. This can be attributed to the effect of different mesoporous structures since the formation of metal nanoparticles is mainly controlled by the architecture of the host material. On MCM-41 and SBA-15, Pd nanoparticles show a high degree of thermal sintering within the straight mesochannels, leading to the migration and coalescence of Pd nanoparticles and thereby the ineffective catalytic performance. The inferior performance of SBA-15 when compared to MCM-41 is due to the interconnected micropores in SBA-15 where Pd nanoparticles may be completely buried and inactive. Although the "super-cage" porosity of SBA-16 is superior for confining metal nanoparticles with high dispersion in a "ship in a bottle" way, which has been previously proven by our group [15,16], the mass diffusion limitation is severe and its inferior catalytic activity is due to the restriction by the diffusion of reactants to active sites during the reaction.

For TUD-1, the mesopores have larger diameter than that of SBA-16 and are randomly interconnected. The tortuous pore arrangements can help to provide sufficient defects to encapsulate and restrict the mobility of nanoparticles that lead to thermal sintering and growth of particles, and prevent the active centers from reactant poisoning. In addition, according to our previous report, TUD-1 with open 3-D mesopore structure and large pore size can effectively decrease the pore diffusion resistance of the reactants. Therefore, it can provide greater access of the reactants to the active sites embedded on the pore wall surface [18]. The excellent catalytic performance of TUD-1-supported Pd catalysts herein again verifies the superiority of the 3-D sponge-like mesostructure of TUD-1. Hence, upon the APS-modification, palladium precursors can be easily adsorbed, and Pd nanoparticles are uniformly embedded in the mesopores of TUD-1 with a specific size distribution. The suppressed mass transfer limitation, enhanced metal–support interaction, and a finely tuned local basicity surrounding the Pd nanoparticles result in a remarkably improved catalytic performance.

It is clear that local surface basicity and Pd nanoparticle size are two vital factors controlling both the catalytic activity (qTOF) and selectivity. Nevertheless, the surface basicity also affects the particle size and size distribution, as well as the dehydrogenation step in the benzyl alcohol oxidation, resulting in the complex and ambiguous explanation of the effect of individual factors and their interaction on the catalytic performance. To facilitate more rigorous interpretation, we employed statistical techniques to develop a second-order polynomial regression model including both linear and quadratic terms to fit the experimental data of two factors (x_1: Pd size, x_2: pH value) and two responses (y_1: qTOF, y_2: selectivity) (see Supporting information). The contour plots of qTOF and selectivity provide a rational examination of the influence of each experimental variable on the responses, as illustrated in Fig. 13. Both contour plots are elliptically shaped, implying the significant interaction between pH and Pd size [47]. It is obvious in Fig. 9a that

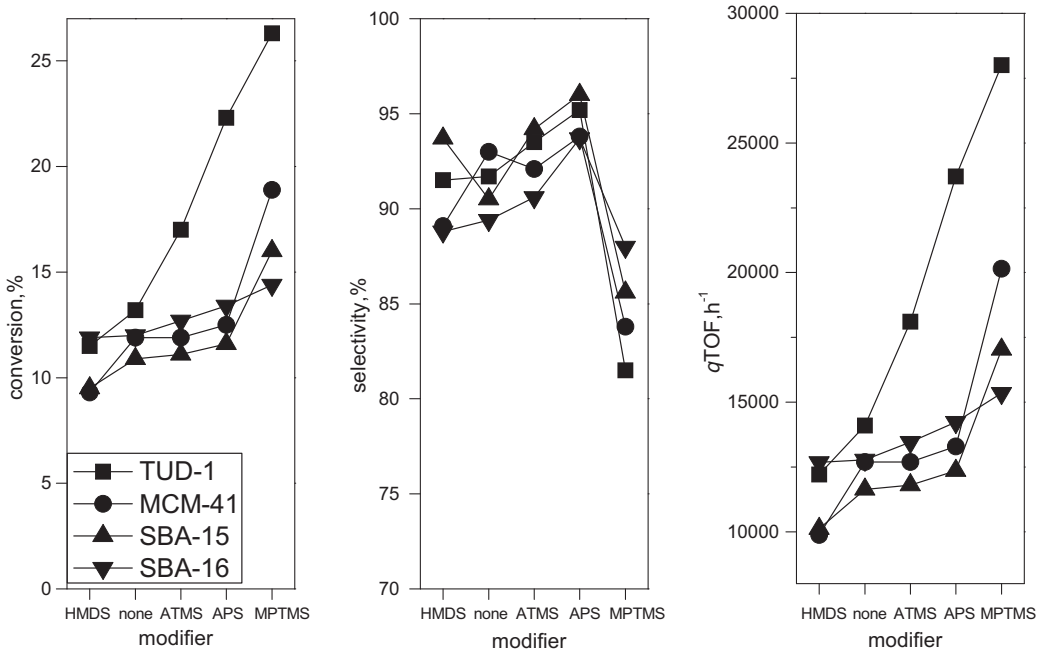

Fig. 12. Catalytic performance of 1 wt.% Pd-containing catalysts supported on pristine and surface-functionalized mesoporous silica supports. Reaction conditions: benzyl alcohol/Pd = 250 mol/g; O_2, 20 mL min^{-1}; temperature, 160 °C; reaction time, 1 h; stirring rate, 1200 rpm.

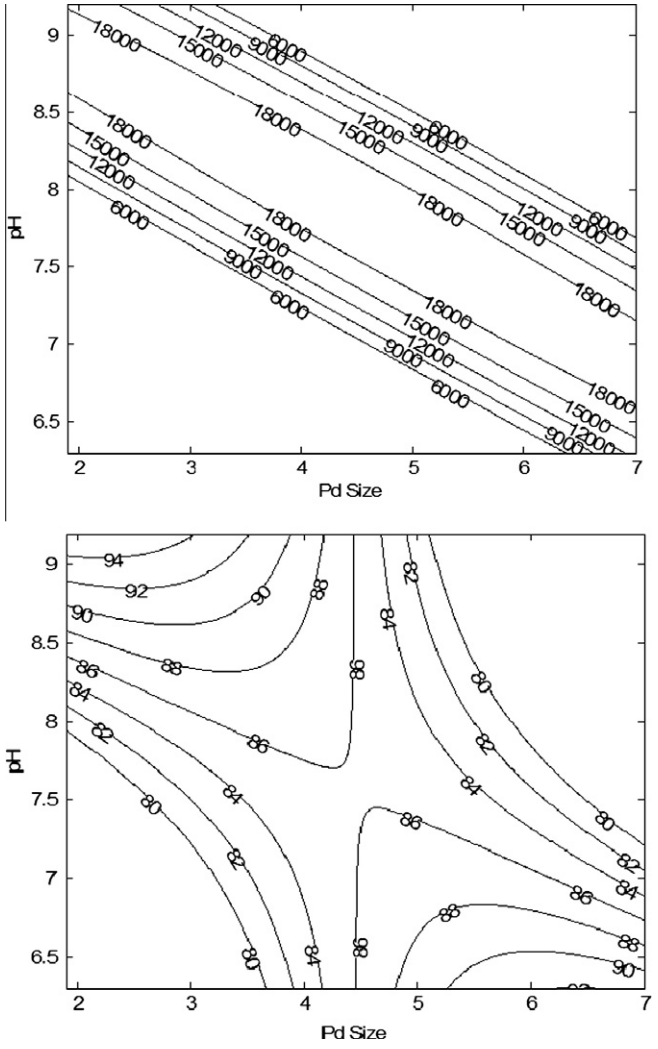

Fig. 13. Contour plots of (a) qTOF and (b) selectivity as a function of Pd size and pH of support.

to obtain high qTOF at small Pd size, the catalyst surface has to be mildly alkaline. Similarly, high selectivity can be achieved at small Pd size and high pH level, and vice versa. Both contour plots reflect similar trend; and therefore, the adjustment of Pd size and surface basicity will affect the catalytic results remarkably. Based on the normalized variables and the improved model (see Supporting information), the prediction formulas of y_1 (qTOF) and y_2 (selectivity) are as follows:

$$y_1 = 19753.3 + 5787.1x_1 + 8196.8x_2 - 21677.9x_1^2 - 43109.2x_2^2 - 60288.2x_1x_2$$

$$y_2 = 85.94 - 2.17x_2 - 10.55x_1^2 - 18.22x_1x_2$$

These quadratic polynomial equations, which were developed to predict the response as a function of the variables and their interactions variables, can be used to determine the catalytic results (qTOF and selectivity) quantitatively and facilitate precise optimization of the reaction parameters.

5. Conclusions

A series of Pd catalysts supported on TUD-1 functionalized with various organosilanes (APS, ATMS, HMDS, and MPTMS) were successfully prepared using a surface-modification scheme followed with a metal adsorption–reduction procedure. The catalytic activities of these as-prepared catalysts were explored in the solvent-free selective oxidation of benzyl alcohol using molecular oxygen. The catalytic results proved that the type and amount of functional group for functionalizing the TUD-1 support showed great impact on the catalytic performance. APS immobilized on TUD-1 with an appropriate amount of APS coverage displayed the best improvement owing to the enhanced metal–support interaction and finely tuned local surface basicity surrounding the Pd nanoparticles. Among all the catalysts, 1Pd/1.2APS-TUD exhibited a dramatically high qTOF of 18,571 h^{-1} for benzyl alcohol conversion. TUD-1 is superior to other mesoporous silicas due to its unique open 3-D sponge-like wide mesostructure, which can effectively confine the nanoparticles and suppress the mass diffusion resistance.

Acknowledgements

We are grateful to AcRF tier 2 (ARC 13/07) for funding support. Authors would also like to acknowledge the great help on discussion and assistance with editing from Professor Gary L. Haller, Yale University.

Appendix A. Supplementary material

Supplementary data associated with this article can be found, in the online version, at doi:10.1016/j.jcat.2010.07.006.

Reference

[1] G.J. Hutchings, Chem. Commun. (2008) 1148.
[2] T.F. Blackburn, J. Schwartz, J. Chem. Soc., Chem. Commun. (1977) 157.
[3] K. Mori, T. Hara, T. Mizugaki, K. Ebitani, K. Kaneda, J. Am. Chem. Soc. 126 (2004) 10657.
[4] F. Li, Q.H. Zhang, Y. Wang, Appl. Catal. A: Gen. 334 (2008) 217.
[5] A.S.K. Hashmi, G.J. Hutchings, Angew. Chem. Int. Ed. 45 (2006) 7896.
[6] T. Mallat, A. Baiker, Chem. Rev. 104 (2004) 3037.
[7] P.J.M. Dijkgraaf, M.J.M. Rijk, J. Meuldijk, K. Vanderwiele, J. Catal. 112 (1988) 329.
[8] S.K. Klitgaard, A.T. DeLa Riva, S. Helveg, R.M. Werchmeister, C.H. Christensen, Catal. Lett. 126 (2008) 213.
[9] J.J. Zhu, J.L. Figueiredo, J.L. Faria, Catal. Commun. 9 (2008) 2395.
[10] C. Bianchi, F. Porta, L. Prati, M. Rossi, Top. Catal. 13 (2000) 231.
[11] D.V. Leff, L. Brandt, J.R. Heath, Langmuir 12 (1996) 4723.
[12] C. Aprile, A. Abad, G.A. Hermenegildo, A. Corma, J. Mater. Chem. 15 (2005) 4408.
[13] C. Bronnimann, T. Mallat, A. Baiker, J. Chem. Soc., Chem. Commun. (1995) 1377.
[14] J.C. Hu, L.F. Chen, K.K. Zhu, A. Suchopar, R. Richards, Catal. Today 122 (2007) 277.
[15] H. Sun, Q.H. Tang, Y. Du, X.B. Liu, Y. Chen, Y.H. Yang, J. Colloid Interface Sci. 333 (2009) 317.
[16] Y. Chen, H. Lim, Q. Tang, Y. Gao, T. Sun, Q. Yan, Y. Yang, Appl. Catal. A: Gen. (2010), doi:10.1016/j.apcata.2010.03.026.
[17] J.C. Jansen, Z. Shan, L. Marchese, W. Zhou, N. von der Puil, T. Maschmeyer, Chem. Commun. (2001) 713.
[18] X.Y. Quek, Q.H. Tang, S.Q. Hu, Y.H. Yang, Appl. Catal. A: Gen. 361 (2009) 130.
[19] Y.S. Chi, H.P. Lin, C.Y. Mou, Appl. Catal. A: Gen. 284 (2005) 199.
[20] F. Kleitz, T.W. Kim, R. Ryoo, Langmuir 22 (2006) 440.
[21] S. Brunauer, P.H. Emmett, E. Teller, J. Am. Chem. Soc. 60 (1938) 309.
[22] E.P. Barrett, L.G. Joyner, P.P. Halenda, J. Am. Chem. Soc. 73 (1951) 373.
[23] S.L. Tian, H. Mo, R.F. Zhang, P. Ning, T.H. Zhou, Adsorption 15 (2009) 477.
[24] P. Horcajada, A. Ramila, F. Gerard, M. Vallet-Regi, Solid State Sci. 8 (2006) 1243.
[25] M.A. Camblor, A. Corma, J. Perezpariente, J. Chem. Soc., Chem. Commun. (1993) 557.
[26] C.A. Koh, R. Nooney, S. Tahir, Catal. Lett. 47 (1997) 199.
[27] Z.H. Luan, J.A. Fournier, J.B. Wooten, D.E. Miser, Micropor. Mesopor. Mater. 83 (2005) 150.
[28] T. Joseph, K.V. Kumar, A.V. Ramaswamy, S.B. Halligudi, Catal. Commun. 8 (2007) 629.
[29] B. Lee, Z. Ma, Z.T. Zhang, C. Park, S. Dai, Micropor. Mesopor. Mater. 122 (2009) 160.
[30] D.I. Enache, J.K. Edwards, P. Landon, B. Solsona-Espriu, A.F. Carley, A.A. Herzing, M. Watanabe, C.J. Kiely, D.W. Knight, G.J. Hutchings, Science 311 (2006) 362.
[31] A. Ramila, B. Munoz, J. Perez-Pariente, M. Vallet-Regi, J. Sol–Gel Sci. Technol. 26 (2003) 1199.
[32] L. Xu, J.H. Fu, J.R. Schlup, J. Am. Chem. Soc. 116 (1994) 2821.
[33] C.C. Perry, X.C. Li, J. Chem. Soc., Faraday Trans. 87 (1991) 761.

[34] X.B. Liu, Y. Du, Z. Guo, S. Gunasekaran, C.B. Ching, Y. Chen, S.S.J. Leong, Y.H. Yang, Micropor. Mesopor. Mater. 122 (2009) 114.
[35] Sujandi, S.E. Park, D.S. Han, S.C. Han, M.J. Jin, T. Ohsuna, Chem. Commun. (2006) 4131.
[36] E. Ozensoy, D.W. Goodman, Phys. Chem. Chem. Phys. 6 (2004) 3765.
[37] P. Hollins, Surf. Sci. Rep. 16 (1992) 51.
[38] Z. Hou, N. Theyssen, A. Brinkmann, K.V. Klementiev, W. Grunert, M. Buhl, W. Schmidt, B. Spliethoff, B. Tesche, C. Weidenthaler, W. Leitner, J. Catal. 258 (2008) 315.
[39] V.Z. Radkevich, T.L. Senko, K. Wilson, L.M. Grishenko, A.N. Zaderko, V.Y. Diyuk, Appl. Catal. A: Gen. 335 (2008) 241.
[40] E.B. Fox, S. Velu, M.H. Engelhard, Y.H. Chin, J.T. Miller, J. Kropf, C.S. Song, J. Catal. 260 (2008) 358.
[41] M.C. Romanmartinez, D. Cazorlaamoros, A. Linaressolano, C.S.M. Delecea, H. Yamashita, M. Anpo, Carbon 33 (1995) 3.
[42] X. Feng, G.E. Fryxell, L.Q. Wang, A.Y. Kim, J. Liu, K.M. Kemner, Science 276 (1997) 923.
[43] Q.H. Tang, Q.H. Zhang, H.L. Wu, Y. Wang, J. Catal. 230 (2005) 384.
[44] C. Keresszegi, D. Ferri, T. Mallat, A. Baiker, J. Phys. Chem. B 109 (2005) 958.
[45] D.M. Meier, A. Urakawa, A. Baiker, J. Phys. Chem. C 113 (2009) 21849.
[46] Q.H. Tang, T. Liu, Y.H. Yang, Catal. Commun. 9 (2008) 2570.
[47] Q.H. Tang, Y.T. Chen, C. Zhou, T. Chen, Y.H. Yang, Catal. Lett. 128 (2009) 210.